Supporting Information

In situ construction of surface oxygen vacancies on N/ TiO_2 for promoting visible-light photocatalytic H_2 evolution

Yuandong Shen [a, 1], Nan Yang [a], Ke Wang [a], Bin Xiao [a, *], Yijun He [a], Zhishi Qiu [a], Tong Zhou [a], Weijie Zhan [a], Rui Hu [a], Genlin Zhang [a, *], Jin Zhang [a], Zhongqi Zhu [a], Feng Liu [b], Hao Cui [b], Qingju Liu [a, *]

[a] Yunnan Key Laboratory for Micro/Nano Materials & Technology, National Center for International Research on Photoelectric and Energy Materials, School of Materials and Energy, Yunnan University, Kunming, 650091, P. R. China.

[b] Yunnan Precious Metals Laboratory Co., Ltd., Kunming, 650106, P. R. China.

[*] Corresponding author: Prof. Qingju Liu, E-mail: qjliu@ynu.edu.cn; Genlin Zhang, E-mail: zhanggenlin@ynu.edu.cn; Bin Xiao, E-mail: ynuxb2011@163.com

Experimental Section

Photocatalysts Preparation

Preparation of NH_2-MIL-125(Ti)

The preparation of NH_2-MIL-125(Ti) was mainly based on the study of Cheng et al. [1]. 36 mL of N,N-Dimethylformamide (DMF) and 4 mL of methanol (MeOH) were successively added to the beaker. After mixed well, 1.385 g of 2-Aminoterephthalic Acid (NH_2-BDC) was added during stirring. After it was completely dissolved, 2.21 mL of acetic acid (AA) was added dropwise and mixed well, followed by a slow drop of 1.185 mL of Titanium(IV) isopropoxide (TPOT). The mixture was ultrasonicated for 10 min and stirred for 2 h, then transferred to a 100 mL reactor and hydrothermally reacted for 24 h at 150 ℃. The reaction was completed to obtain a yellow precipitate, which was washed three times with DMF and methanol, respectively. Finally, it was vacuum dried at 80 ℃ for 5 h to obtain the octahedral type NH_2-MIL-125(Ti).

Preparation of N-doped TiO_2 and X-N/TiO_2

According to the research of Gao et al. [2], N-doped TiO_2 (N/TiO_2) can be prepared by direct sintering of NH_2-MIL-125(Ti). Therefore, we increased the prepared NH_2-MIL-125(Ti) at an elevated temperature rate of 2 °C/min to 550 °C and held it for 6 h. The product was named N/TiO_2. We then constructed oxygen vacancies in situ on the surface of N/TiO_2. Firstly, thiourea with a mass ratio of X to NH_2-MIL-125(Ti) was taken into a beaker and 15 mL of deionized water was added for dissolution (X is 0.8, 1, 1.2, 1.4, 1.6). Secondly, 200 mg of the prepared NH_2-MIL-125(Ti) was added to the above thiourea solution, sonicated for 10 min and then evaporated to dryness in a 60 °C water bath with stirring. Thirdly, the obtained powder was evenly ground, transferred to a crucible and calcined at 550 ℃ for 6 h in air at an elevated temperature rate of 2 ℃/min. Finally, the resulting powder was washed three times with deionized water and vacuum dried at 60 ℃ for 5 h to obtain N-doped TiO_2 with surface oxygen vacancies.

The samples were named X-N/TiO_2 based on the different ratios of thiourea to NH_2-MIL-125(Ti). Pure anatase TiO_2 was prepared using a patented method previously developed by our group [3, 4]. Under the condition of 60 ℃ water bath, 5 mL of tetrabutyl titanate was slowly dropped into a mixed solution of 75 mL of deionized water and 3 mL of hydrolysis inhibitor. Adjusted the pH of the solution to 2-3 and stirred for 6-8 h until the turbid solution became transparent and clear. After drying at 60 °C, the obtained powder was calcined at 400 °C for 2 h. Finally, the obtained powder was ground to obtain pure TiO_2.

Characterization

The X-ray diffraction pattern (XRD) was obtained by Cu-Kα radiation on the X-ray diffractometer (TTRIII Rigaku, Japan) to determine the phase structure of the sample (the accelerating voltage and applied current were 40 kV and 80 mA, respectively). The microstructure of the sample was observed by transmission electron microscope (TEM, JEM-2100). X-ray photoelectron spectroscopy (XPS) was measured by a photoelectron spectrometer (Thermo ESCALAB 250Xi, USA) with an Al Kα radiation source (hν =1486.6 eV). The full spectrum scanning energy was 100 eV with a step size of 1 eV, and the fine spectrum scanning energy was 50 eV with a step size of 0.1 eV. The binding energy was corrected by surface contamination C 1s (284.8 eV). Ti K-edge XAS spectra were collected on the RapidXAFS 2 M (Anhui Absorption Spectroscopy Analysis Instrument Co., Ltd., China). The UV-Vis diffuse reflectance spectra were obtained via the diffuse reflectance spectra (DRS) measured on the ultraviolet-visible spectrophotometer (Shimadzu, UV-2600, Japan). Steady-state photoluminescence (PL) was obtained by direct detection of powder samples with a fluorescence spectrometer (FL4500, Shimadzu, Japan) with an excitation wavelength of 375 nm. The lifetime of photogenerated carriers for the sample was obtained by time-resolved fluorescence decay (TRPL) spectroscopy (FLS1000, UK). Electron paramagnetic resonance (EPR) spectroscopy was carried out on Bruker ESR5000 (Bruker BioSpin GmbH, Germany). Under the condition of the same test parameters (9.4548 GHz, 10 dB), mass (20 mg)

and argon (Replace the air in the glass tube containing the sample with high-purity argon gas 20 times), the unpaired electrons in the powder samples were detected by EPR at room temperature. The in situ EPR test conditions were consistent with the above. Specifically, after testing the conventional EPR of the sample, the glass tube containing the sample was then irradiated under a 300 W xenon lamp for 30 min and tested again.

Evaluation of Catalytic Performance

The photocatalytic water-splitting experiments were carried out on a multi-channel photochemical reaction test system with a 5 W LED lamp (PCX-50C Discover, Perfect Light Ltd.). Under magnetic stirring, 5 mg catalyst was uniformly dispersed in a closed reaction bottle containing a mixture of 30 mL water and methanol (H_2O: methanol = 3:1, reactor volume is 50 mL). Then the air in the reaction bottle was replaced with high-purity argon 20 times under stirring, and the pressure was adjusted to 30 kPa. Finally, the reaction bottle was installed on PCX-50C Discover for testing, and the test temperature was kept at 40 °C. The cycle stability test was also carried out under the same condition. Considering the accelerated volatilization of methanol in vacuum and this temperature, methanol was replenished after each cycle (3 hours) to the same level as the first cycle to ensure that the experimental conditions are the same in each cycle. And then, repeat the above operation until the end of the cycle test. The apparent quantum efficiency (AQE) was measured on the same test system and the same condition.

AQE is calculated from the hydrogen production rate obtained from formula (1) [5] and single-wavelength LED lamp (PCX-50C, 5 W). The wavelengths of monochromatic light are 365 nm, 385 nm, 400nm and 420 nm, respectively. The corresponding light intensity are 116.9 mW/cm^2, 147.6 mW/cm^2, 72.1 mW/cm^2 and 51.4 mW/cm^2, respectively.

$$AQE = \frac{2MN_A hc}{AIt\lambda} \times 100\% \qquad (1)$$

where M is the molar amount of hydrogen, N_A is the Avogadro's constant, h is the Planck constant, c is the speed of light, I is the intensity of light, A is the irradiation area, t is the reaction time, and λ is the wavelength of light.

Photo-electrochemical Measurements

The sample (2 mg) was added to the mixed solution of 0.5 mL ethanol and 20 μL Nafion solution (5 wt%). The prepared samples were uniformly coated on indium-tin-oxide (ITO) slides (2.0 cm × 2.0 cm) and dried at 60 °C for 1 h to prepare working electrodes. The photo-electrochemical properties of the electrodes were measured by CHI-760E electrochemical workstation in a three-electrode system. Pt electrode and Ag/AgCl electrode were used as auxiliary electrode and reference electrode, respectively. The electrolyte was 0.2 M of Na_2SO_4 aqueous solution and the Xe-lamp was 150 W. The photocurrent of the electrodes was measured using the amperometric (I-t curve) technique under repeatedly interrupted light irradiation. Electrochemical impedance spectroscopy (EIS) measurements were carried out under the applied voltage of 5.0 mV, and the frequency range was 10^5-0.1 Hz.

Computational Details

In this work, the Vienna Ab initio simulation package (VASP) was used for density flood theory (DFT) calculations. The Perdew-Burke-Erzenhoff (PBE) [6] of generalized gradient approximation (GGA) [7] function is employed for the treatment of exchange-correlation interactions. The projection-enhanced wave (PAW) [8] potential is used to characterize the interaction between valence electrons and nuclei. 2×2×1 gamma-centered Monkhorst-Parker k-point grid is used for Brillouin zone integration [9]. DFT+U (U-J=7.8-1) for Ti atoms is used to solve the underestimated TiO_2 band gap and correct the interaction between atoms. For the energy received by the atom and the convergence of the force are set to 1×10^{-5} eV and 0.05 eV/Å, respectively. According to XRD patterns, we conducted (101) section of anatase TiO_2 to construct 44 atoms in 4 O-Ti-O atomic layers. To better simulate the real environment, we fixed the bottom

two atomic layers, a total of 72 atoms. The lattice parameters of TiO_2 (101) are a=10.21 Å and b=11.33 Å, respectively. The lattice length in the z-direction was set to be 27.86 Å to ensure that there was sufficient vacuum thickness between the slabs.

The effect of the active site on the hydrogen evolution performance of the TiO2 system was investigated by calculating the corresponding Gibbs free energy. All calculations are based on the computational hydrogen electrode (CHE) proposed by Nørskov et al[10]. The Gibbs free energy of the proton and electron pair (h+ + e-) is equal to half of the free energy of gaseous hydrogen (H2). In addition, the free energy of the H atom is corrected at 298.15 K. Finally, VASPKIT[11] was used to post-process the computational results.

Supporting Figures

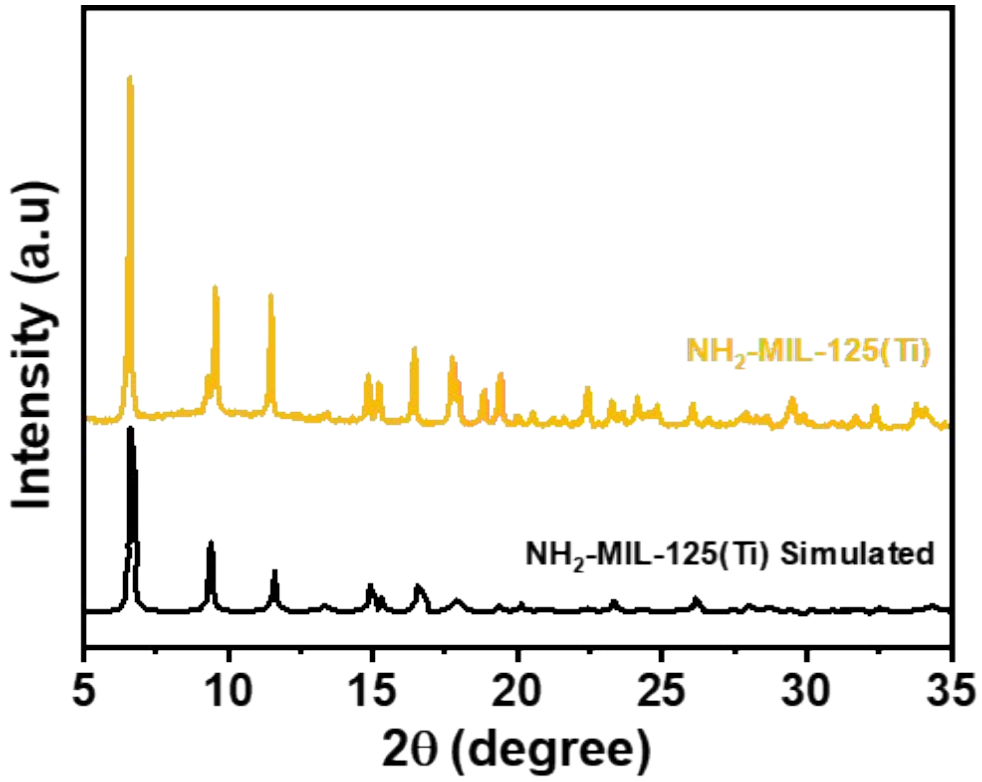

Figure S1. XRD patterns of as-synthesized NH_2-MIL-125(Ti) and simulated NH_2-MIL-125(Ti).

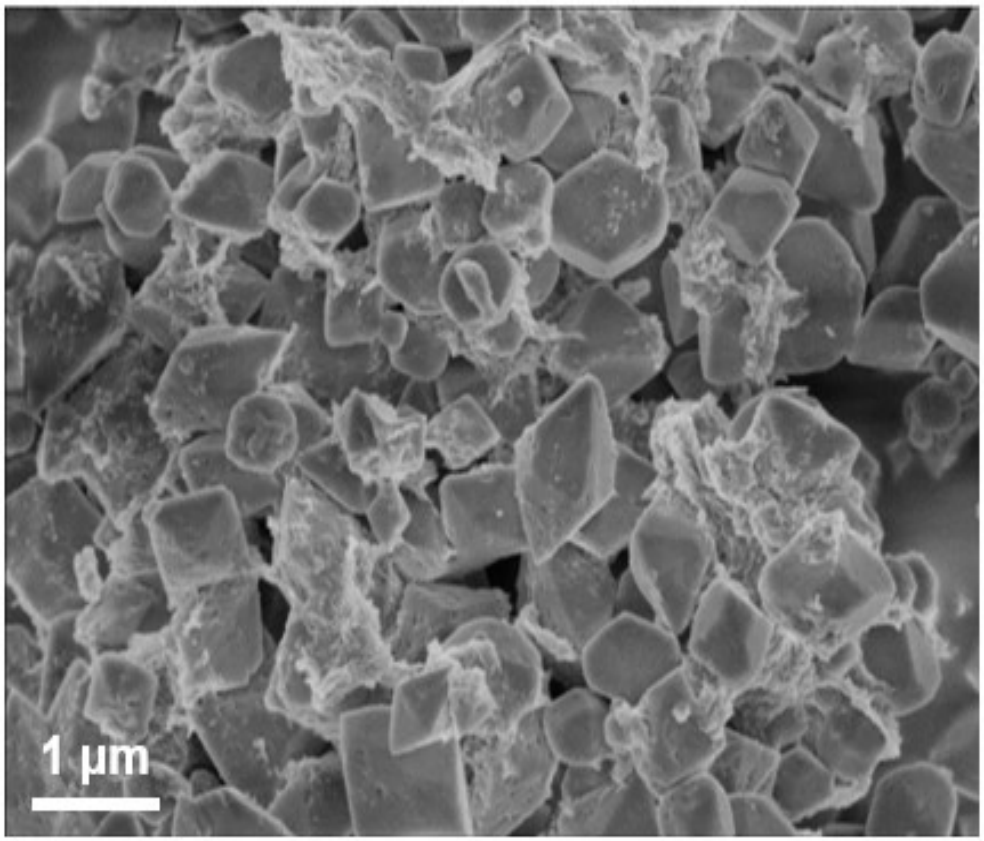

Figure S2. SEM spectra of NH_2-MIL-125(Ti).

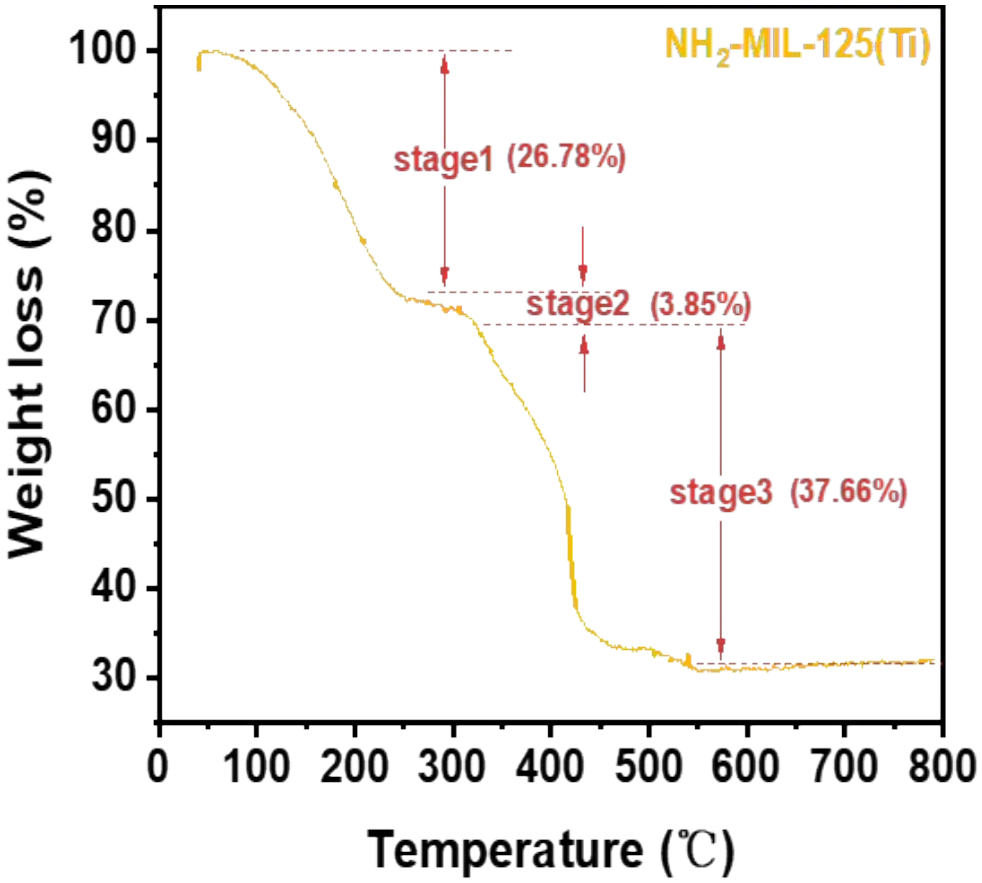

Figure S3. TGA curve of NH_2-MIL-125(Ti) in air atmosphere.

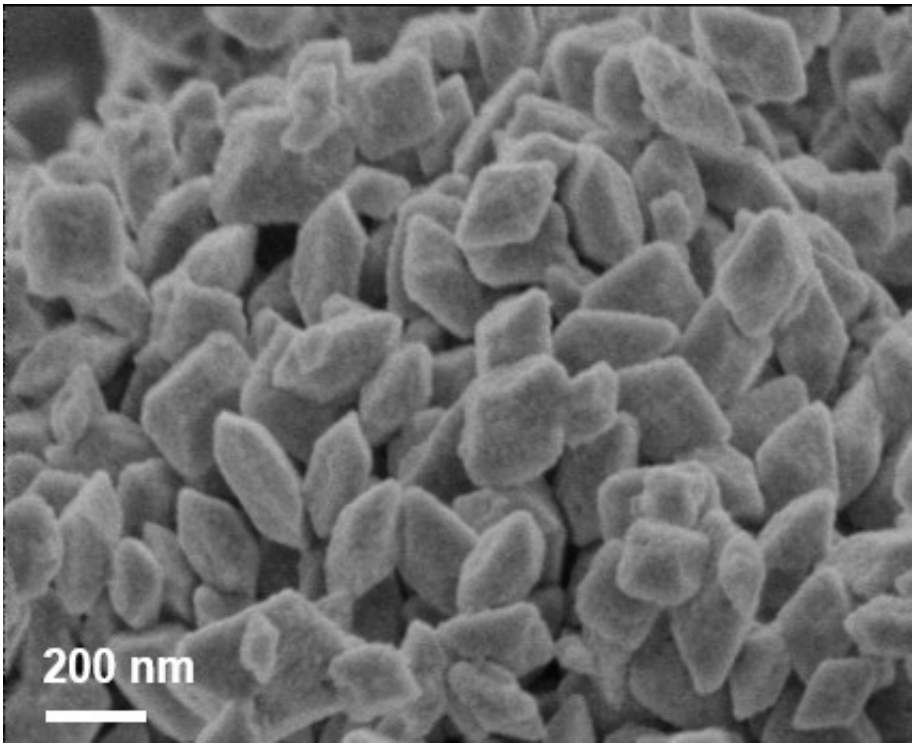

Figure S4. SEM spectra of N/TiO_2.

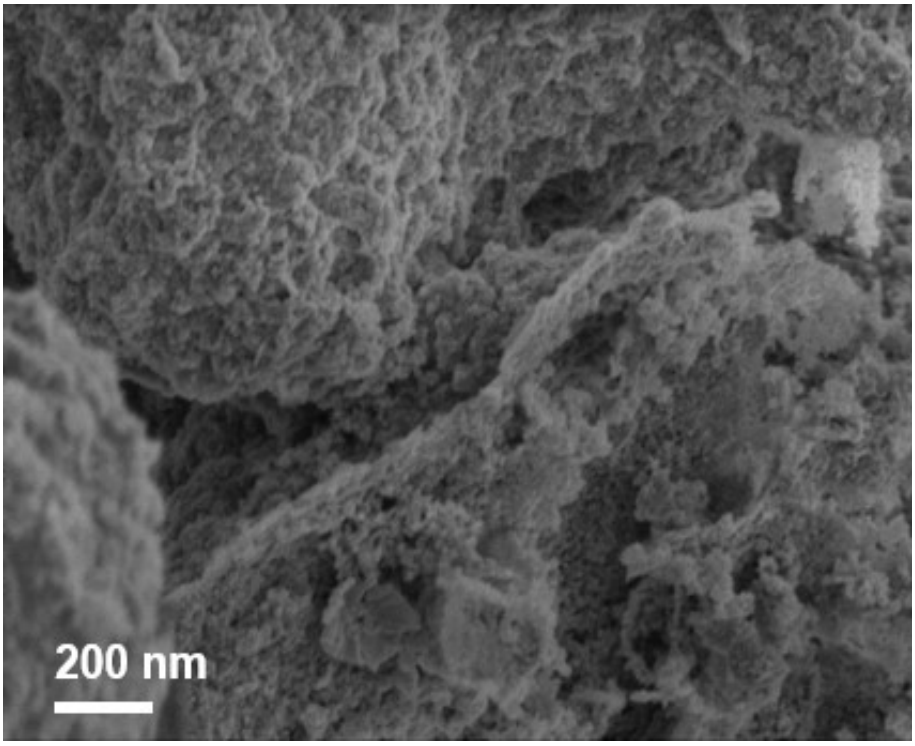

Figure S5. SEM spectra of 1.2-N/TiO_2.

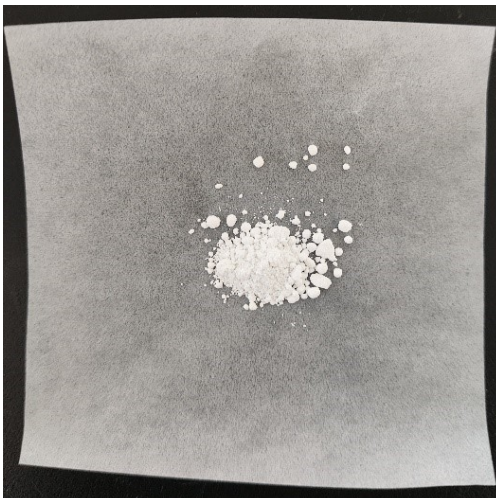

Figure S 6. TiO_2 powder.

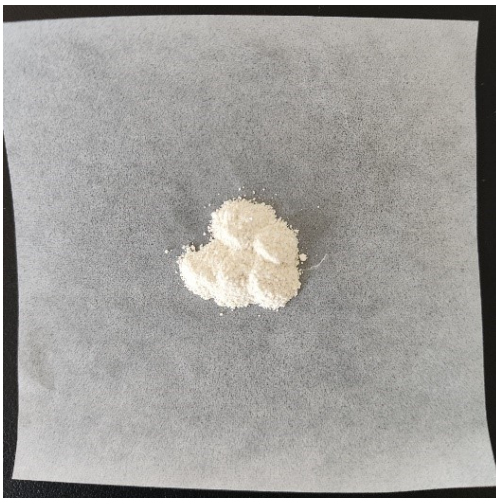

Figure S7. N/TiO_2 powder.

Figure S8. 1.2-N/TiO_2 powder.

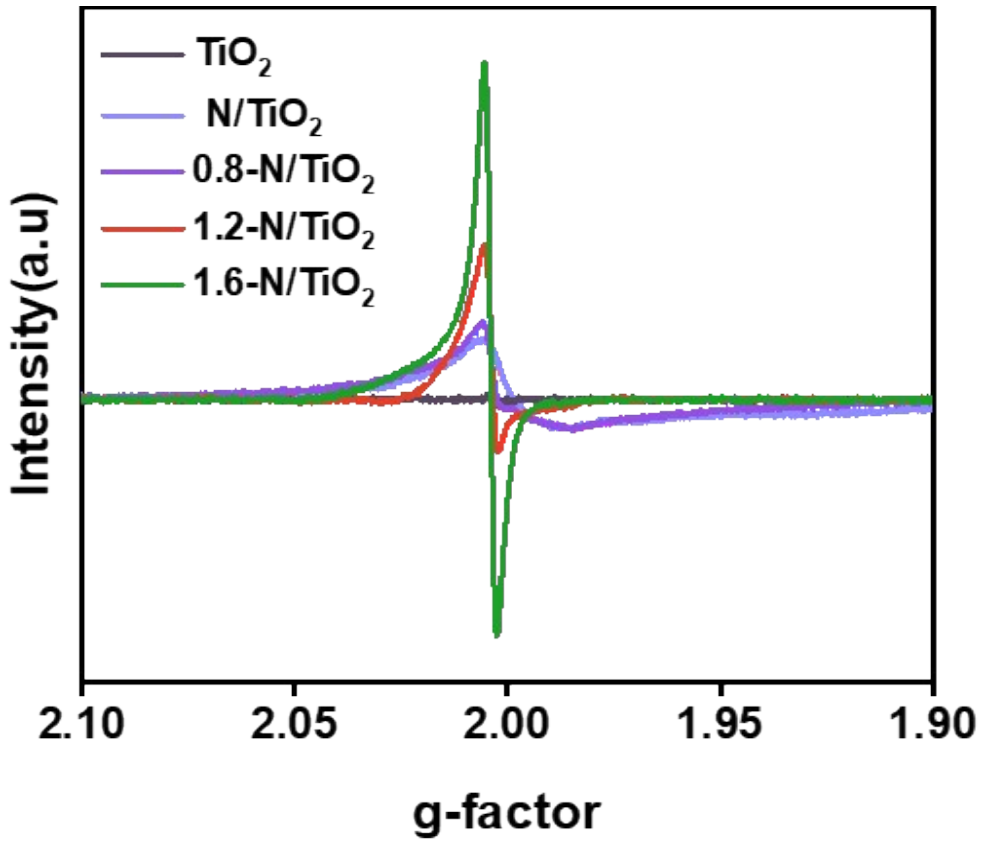

Figure S9. EPR spectra of TiO_2, N/TiO_2, 0.8-N/TiO_2, 1.2-$N/TiO_2$and 1.6-N/TiO_2.

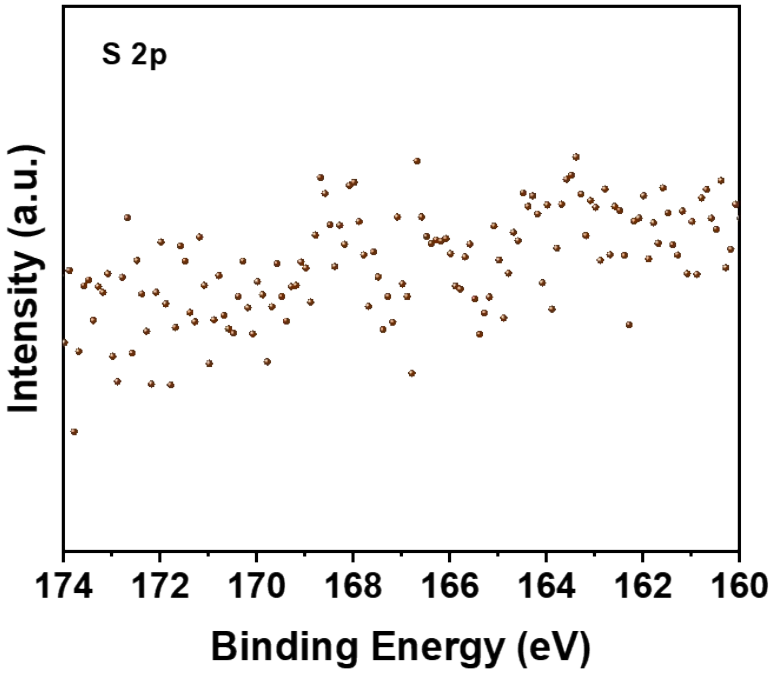

Figure S 10. XPS spectra of S 2p of 1.2-N/TiO_2.

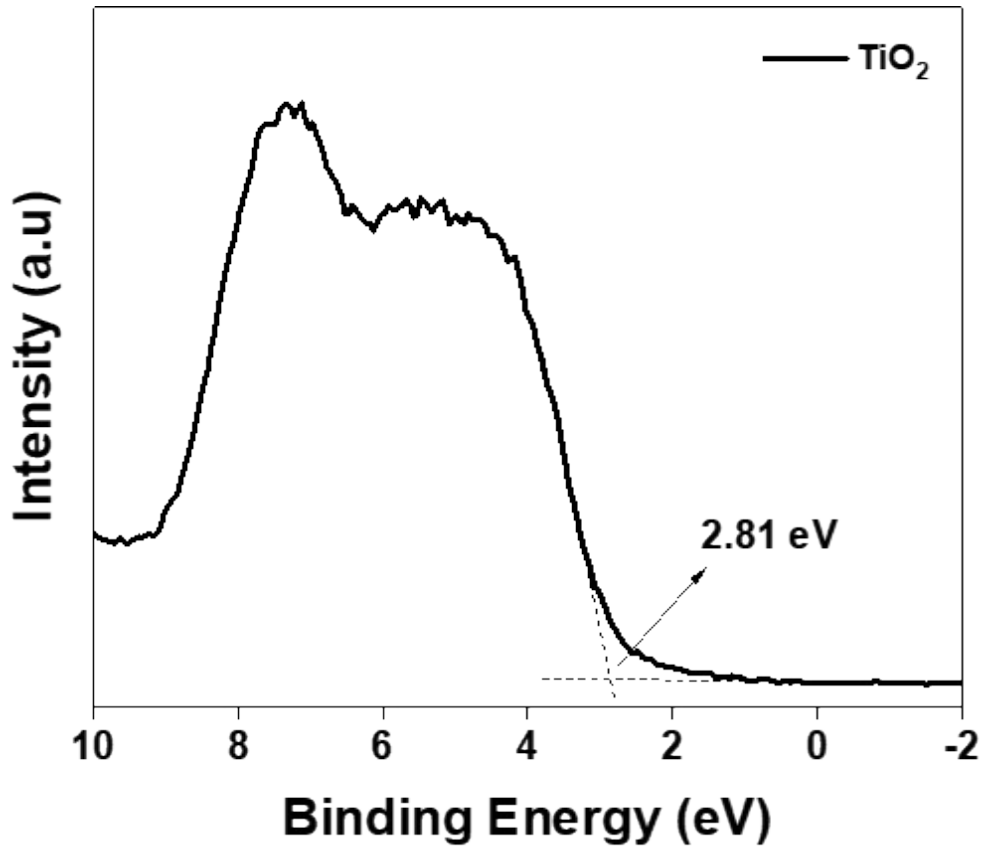

Figure S11. valence band XPS spectrum of TiO_2.

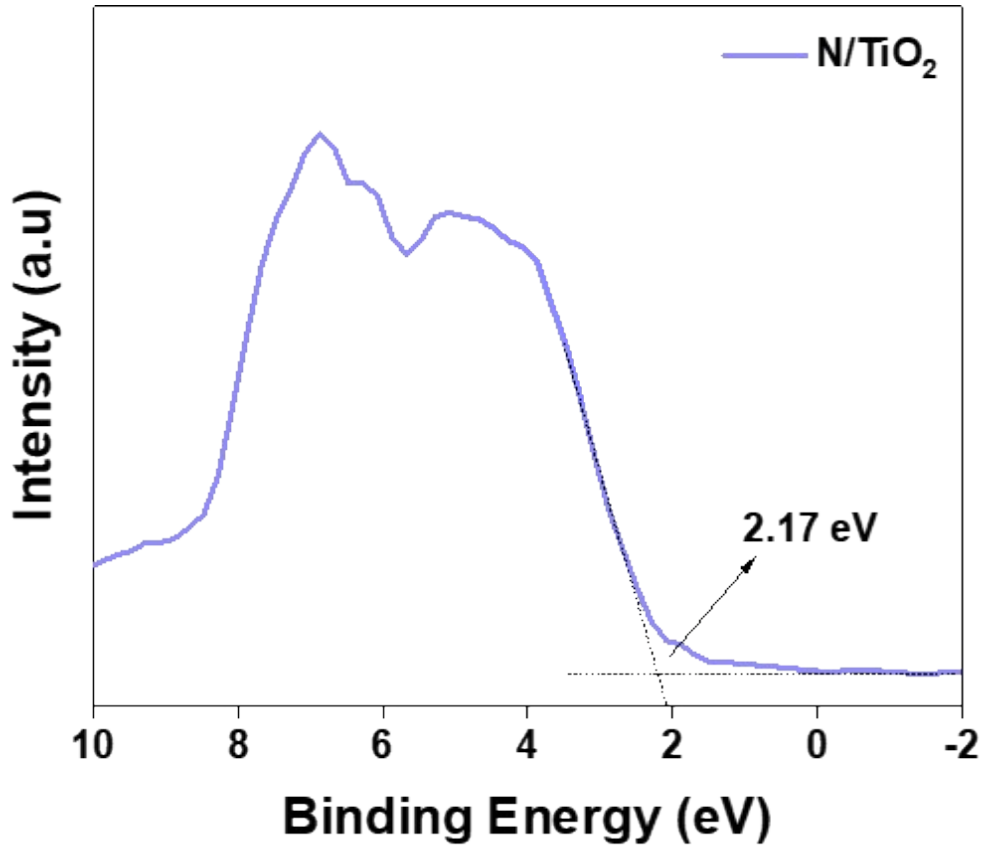

Figure S12. valence band XPS spectrum of N/TiO_2.

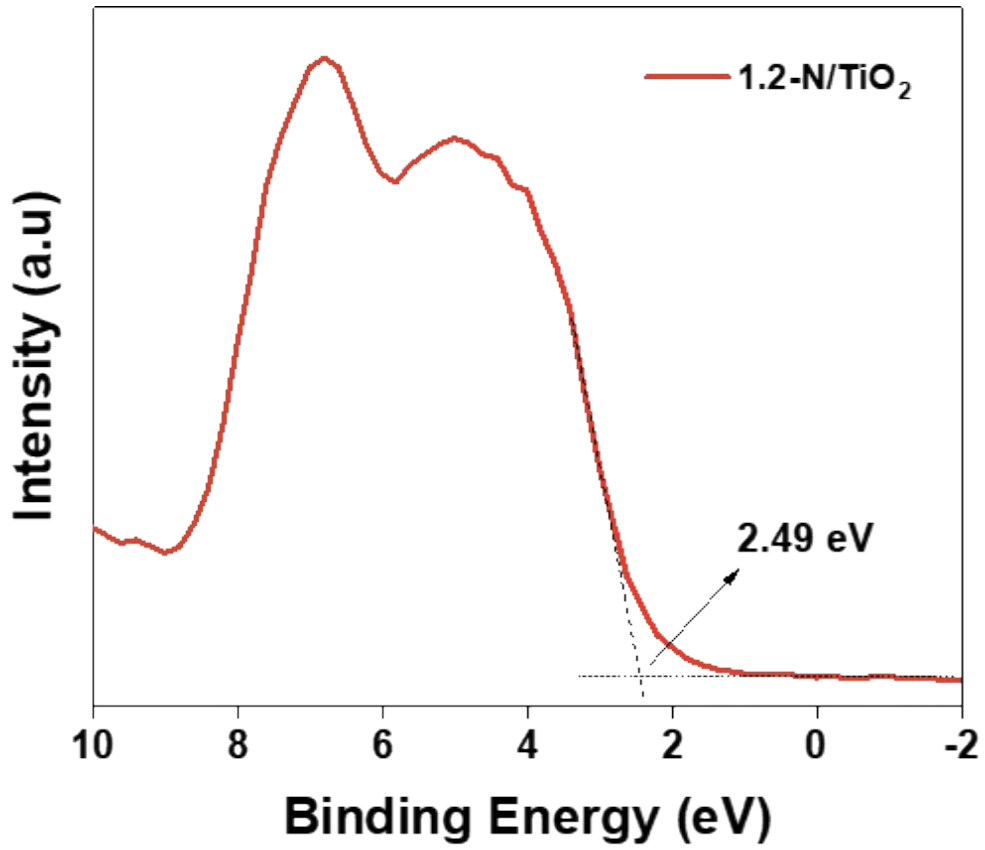

Figure S13. valence band XPS spectrum of 1.2-N/TiO_2.

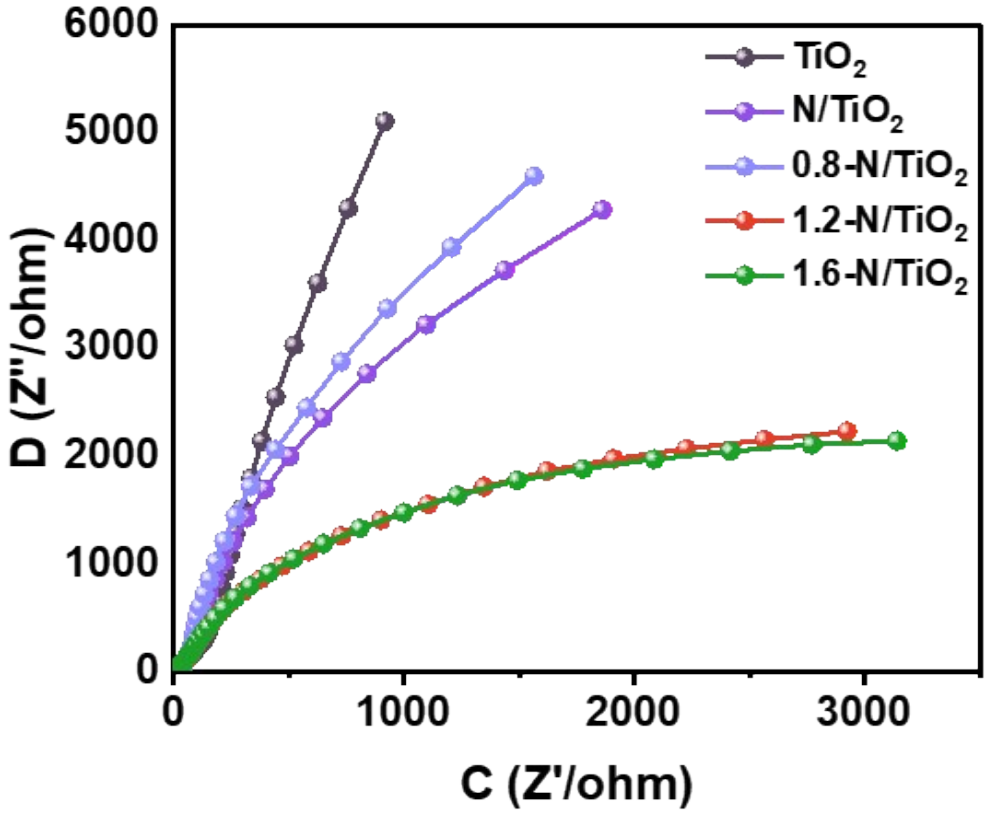

1

2 Figure S14. EIS curves of TiO_2, N/TiO_2, $0.8\text{-}N/TiO_2$, $1.2\text{-}N/TiO_2$and $1.6\text{-}N/TiO_2$.

3

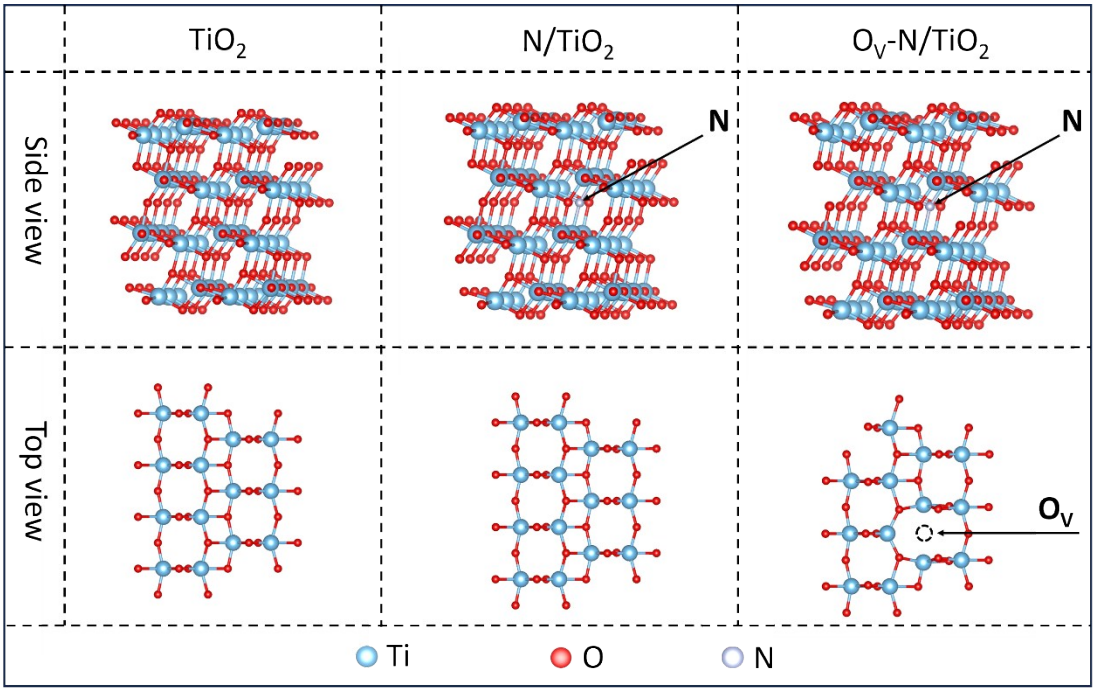

Figure S15. Model structures for pristine TiO_2, N/TiO_2 and N/TiO_2-O_V.

Table S1 The compositions of as-prepared TiO_2 nanocrystals derived from XPS analyses.

Sample	Composition (at%)				
	Ti [a]	O [b]	O [c]	N [d]	C [e]
N/TiO_2	23.43	46.38	4.37	0.81	25.01
$1.2\text{-}N/TiO_2$	24.43	42.03	8.23	0.61	24.85

[a] Ti at% from the Ti - O bond.

[b] O at% from the Ti - O bond.

[c] O at% from the adsorbed oxygen.

[d] N at% from the N - Ti - O bond.

[e] C at% from the C – C and C - O bond.

Table S2 Fitting parameters of the time-resolved photoluminescence decay curves of samples, by the bi-exponential kinetic function.

Sample	A_1(%)	τ_1 (ns)	A_2(%)	τ_2 (ns)	τ_{ave} (ns)
1.6-N/TiO_2	16.59	1.36	0.21	7.34	1.73
1.2-N/TiO_2	0.25	2.36	1.17	14.86	14.45
0.8-N/TiO_2	7.53	1.5	0.61	14.51	7.39
N/TiO_2	11.75	1.39	0.2	5.4	1.28
TiO_2	4.42	1.04	0.17	5.78	1.42

The t for each sample was calculated using the following equation:

$$\tau_{ave} = (A_1\tau_1^2 + A_1\tau_1^2) / (A_1\tau_1 + A_1\tau_1) \quad (2)$$

References

1. Y. X. Zhao, Y. F. Zhao, R. Shi, B. Wang, G. I. N. Waterhouse, L. Z. Wu, C. H. Tung and T. R. Zhang, *Adv. Mater.*, 2019, **31**, 9.
2. Q. Gao, L. Sun, Z. H. Wang and J. G. Deng, *Chin. Chem. Lett.*, 2024, **35**, 4.
3. T. P. Lv, J. H. Zhao, M. P. Chen, K. Y. Shen, D. M. Zhang, J. Zhang, G. L. Zhang and Q. J. Liu, *Materials*, 2018, **11**, 12.
4. H. L. Gao, J. M. Liu, J. Zhang, Z. Q. Zhu, G. L. Zhang and Q. J. Liu, *Chin. J. Catal.*, 2017, **38**, 1688-1696.
5. Y. F. Zhao, H. Zhou, X. R. Zhu, Y. T. Qu, C. Xiong, Z. G. Xue, Q. W. Zhang, X. K. Liu, F. Y. Zhou, X. M. Mou, W. Y. Wang, M. Chen, Y. Xiong, X. G. Lin, Y. Lin, W. X. Chen, H. J. Wane, Z. Jiang, L. R. Zheng, T. Yao, J. C. Dong, S. Q. Wei, W. X. Huang, L. Gu, J. Luo, Y. F. Li and Y. E. Wu, *Nat. Catal.*, 2021, **4**, 134-143.
6. V. Milman, B. Winkler, J. A. White, C. J. Pickard, M. C. Payne, E. V. Akhmatskaya and R. H. Nobes, *International Journal of Quantum Chemistry*, 2000, **77**, 895-910.
7. M. Ernzerhof and J. P. Perdew, *The Journal of Chemical Physics*, 1998, **109**, 3313-3320.
8. G. Kresse and D. Joubert, *Physical Review B*, 1999, **59**, 1758-1775.
9. S. Froyen, *Phys Rev B Condens Matter*, 1989, **39**, 3168-3172.
10. B. Hammer and J. K. Norskov, *Surface Science*, 1995, **343**, 211-220.
11. V. Wang, N. Xu, J.-C. Liu, G. Tang and W.-T. Geng, *Computer Physics Communications*, 2021, **267**.